Electronic Supplementary Information

Vesicular Assemblies of Thermoresponsive Amphiphilic Polypeptide Copolymers for Guests Encapsulation and Release

Mahammad Anas, Somdeb Jana and Tarun K. Mandal*

School of Chemical Sciences, Indian Association for the Cultivation of Science, Jadavpur, Kolkata 700032, India

Contents **Page No.**

Synthesis of 2-Isopropyl-2-oxazoline (^{i}POx)

At first zinc acetate dihydrate (2.86 g, 13.02 mmol) and isobutyronitrile (39 mL, 434.1 mmol) were taken in a 50 mL RB flask and heated at 120 °C for few minutes. Ethanolamine (31.5 mL, 520.9 mmol) was then added dropwise while refluxing the mixture at that particular temperature for 24 h. After that the whole solution was washed 3 times with water and 2 times with DCM and finally distilled under reduce pressure to collect a colourless pure liquid product with almost 60% yield. The details characterization data, ESI-MS (Figure S11), ^{1}H-NMR (Figure S12) and ^{13}C-NMR (Figure S13) were given below.

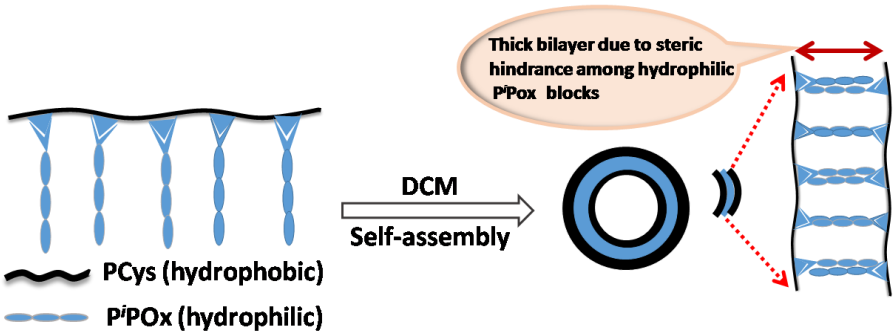

Scheme S1. Schematic representation for the formation of vesicles by polypeptide copolymer in DCM

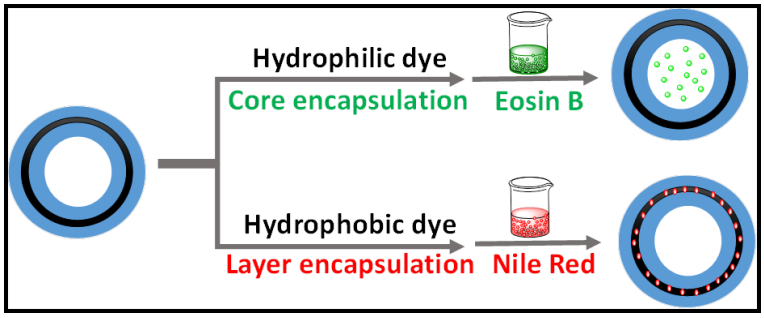

Scheme S2. Schematic representation for the encapsulation behaviours of different dyes by the as-synthesized graft copolymer vesicles in water.

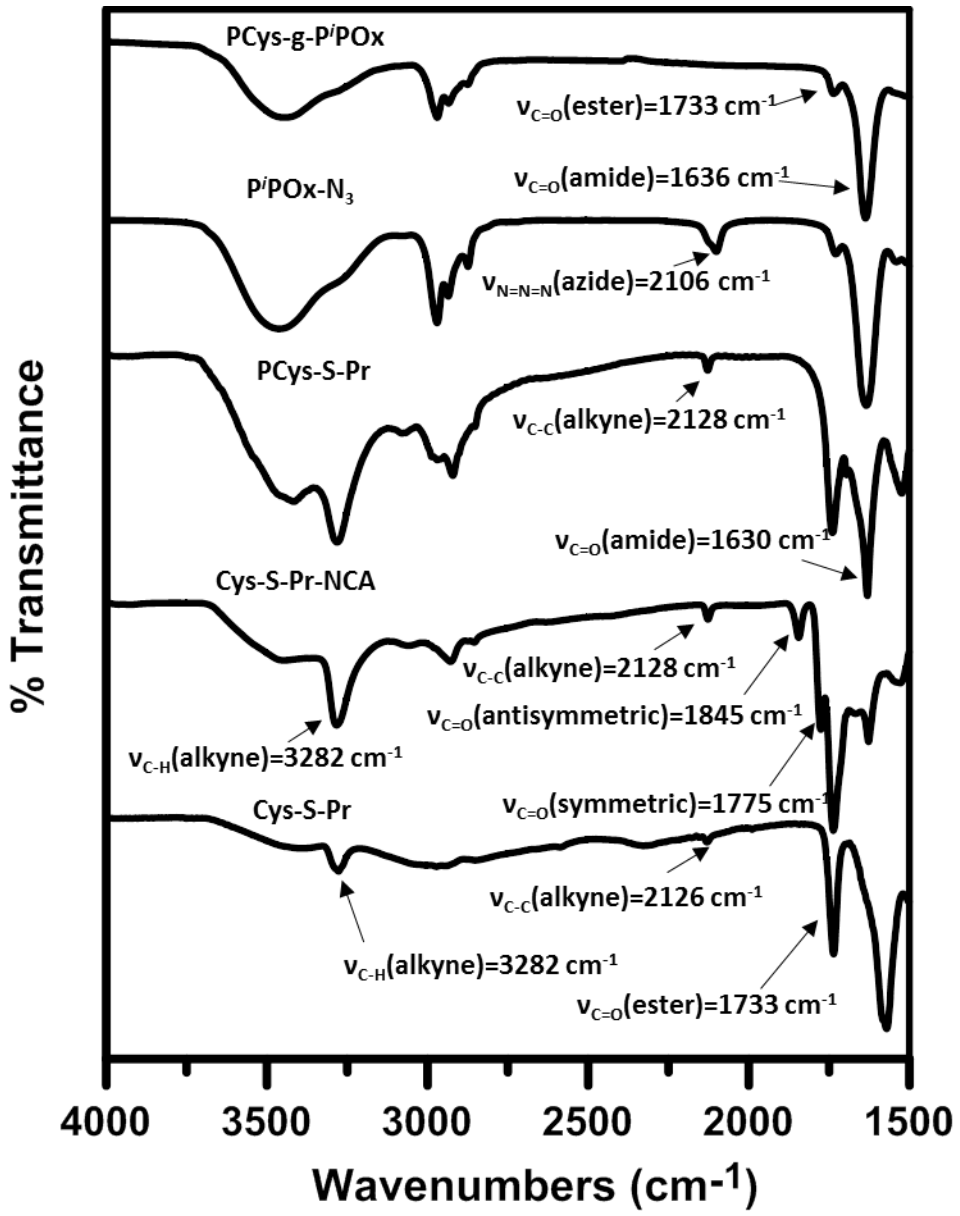

Figure S1. FTIR spectra of all the compounds.

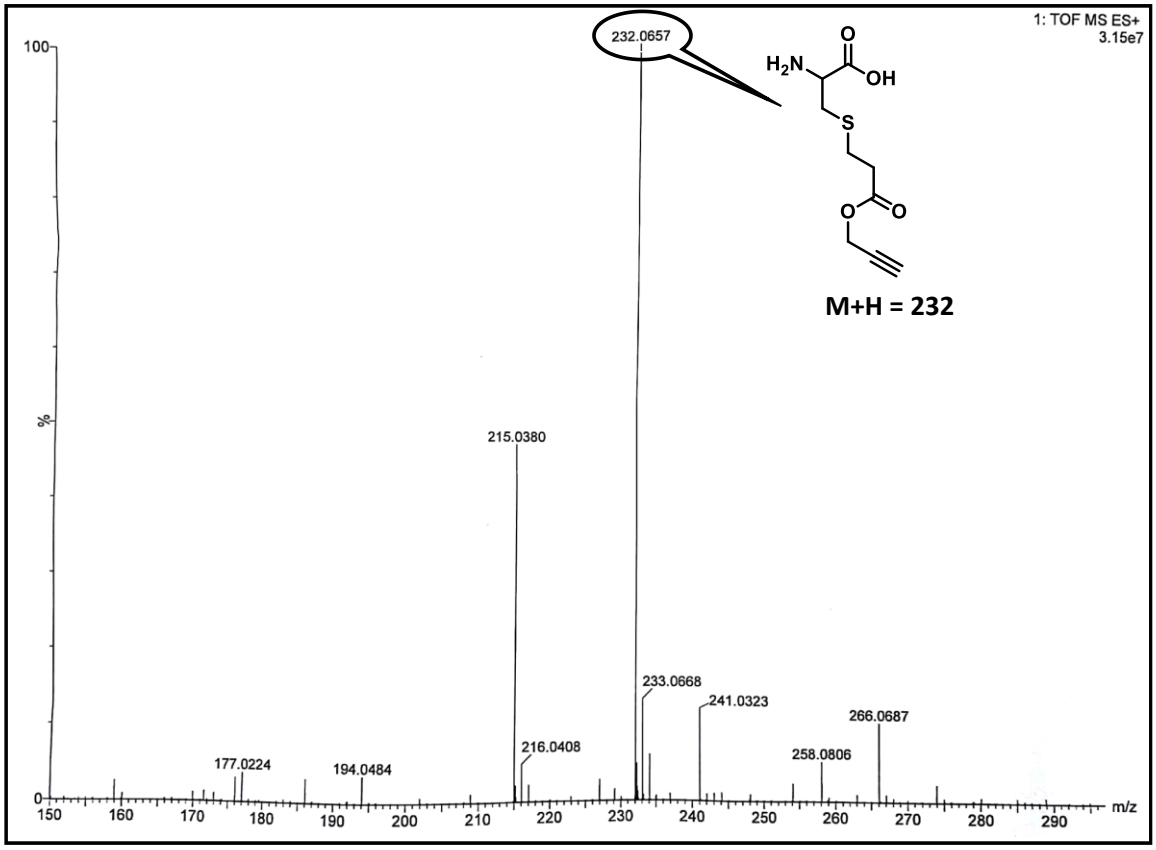

Figure S2. ESI-MS spectrum of Cys-S-Pr in mixture of MeOH: H_2O (1:1)

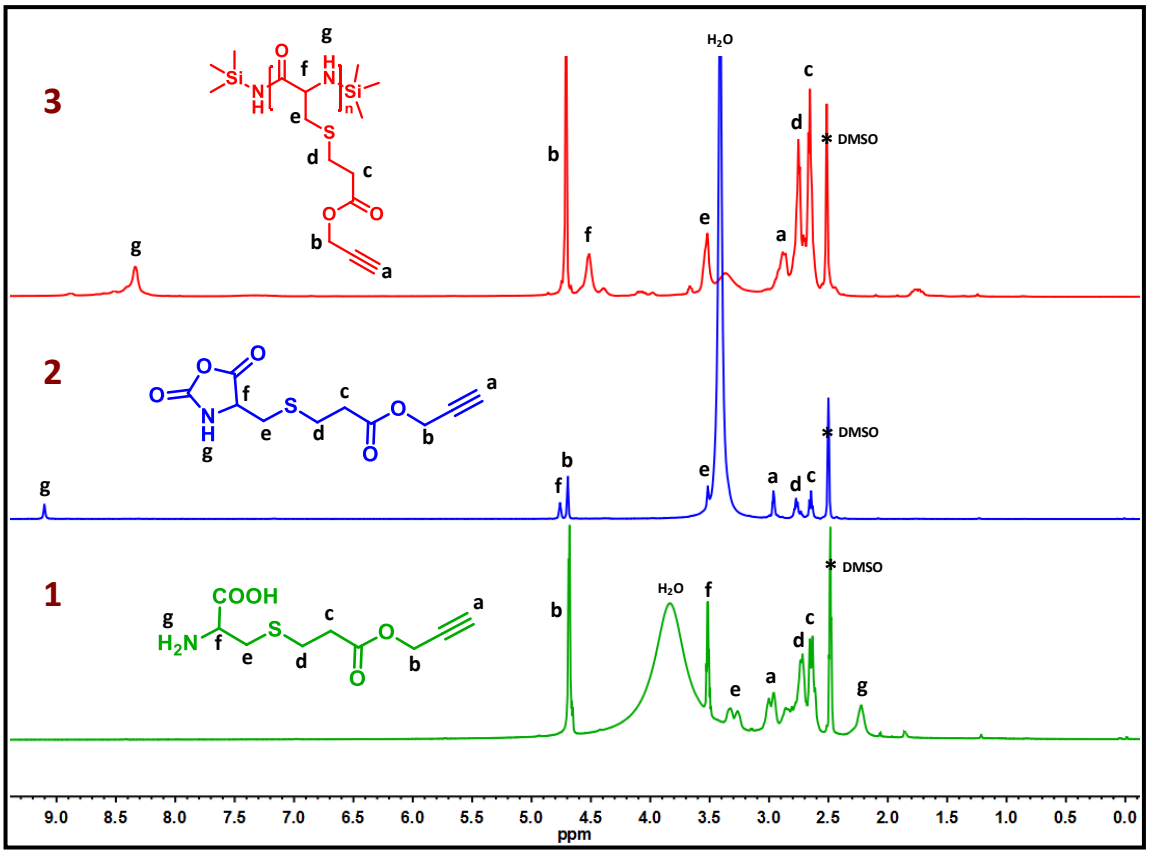

Figure S3. ^{1}H-NMR spectra of Cys-S-Pr (1), Cys-S-Pr NCA (2), PCys-S-Pr (**C2**) (3) in DMSO-d_6

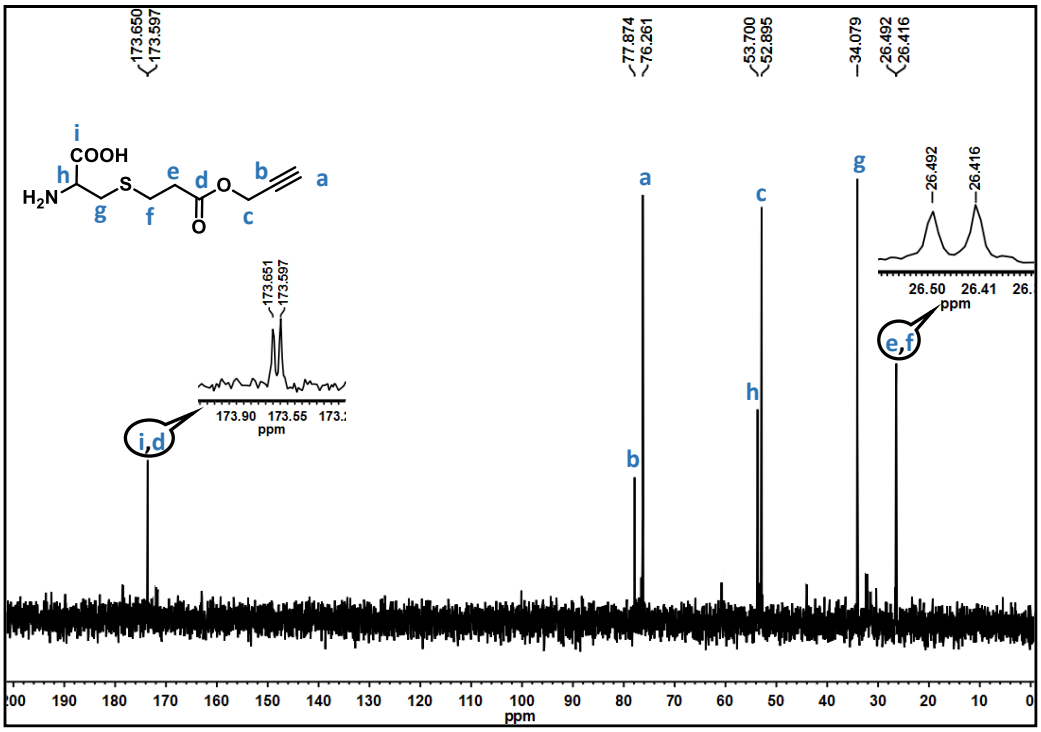

Figure S4. ^{13}C-NMR spectrum of Cys-S-Pr in D_2O

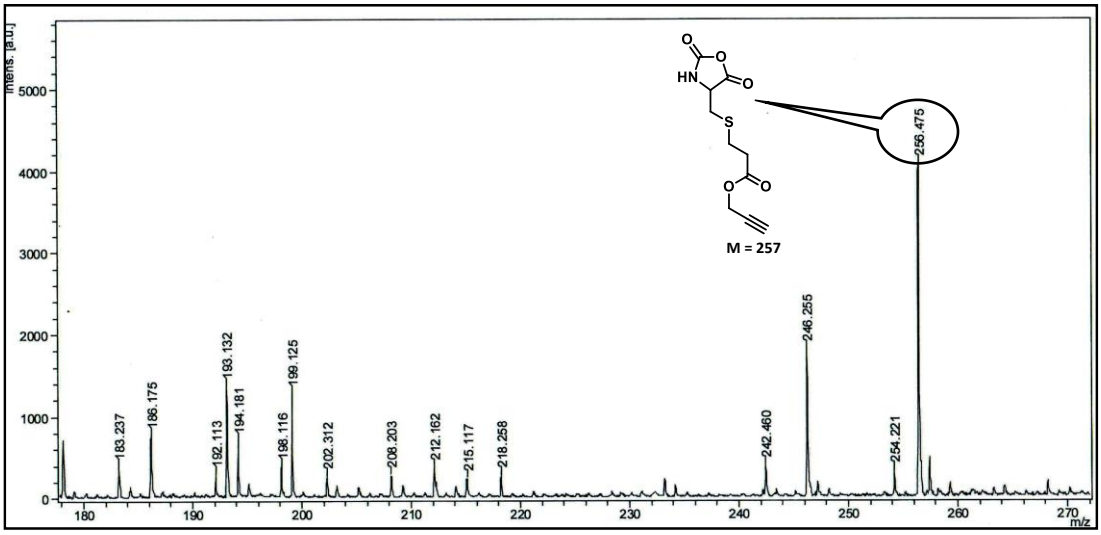

Figure S5. MALDI-TOF-MS spectrum of Cys-S-Pr NCA

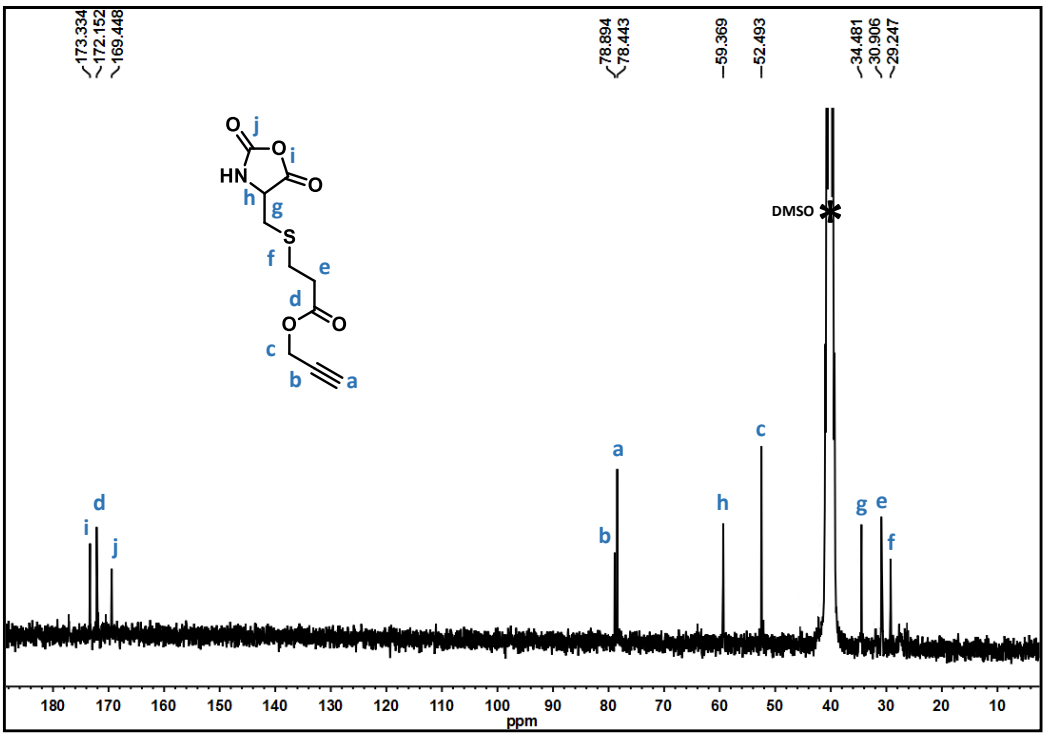

Figure S6. ^{13}C-NMR spectrum of Cys-S-Pr NCA in DMSO-d_6

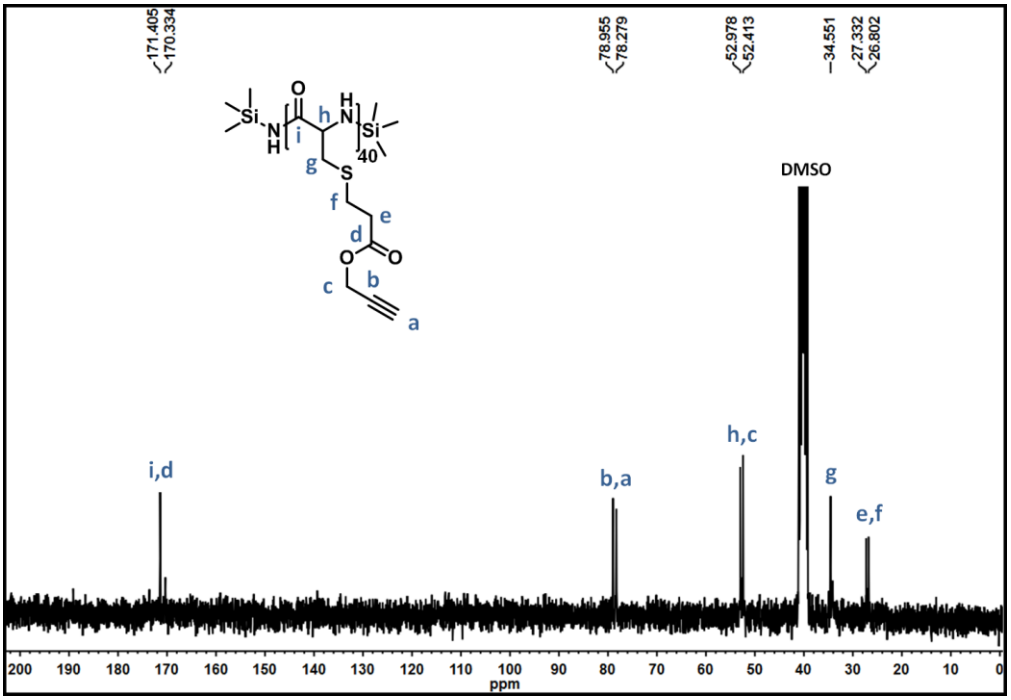

Figure S7. ^{13}C-NMR spectrum of PCys-S-Pr (**C2**) in DMSO-d_6

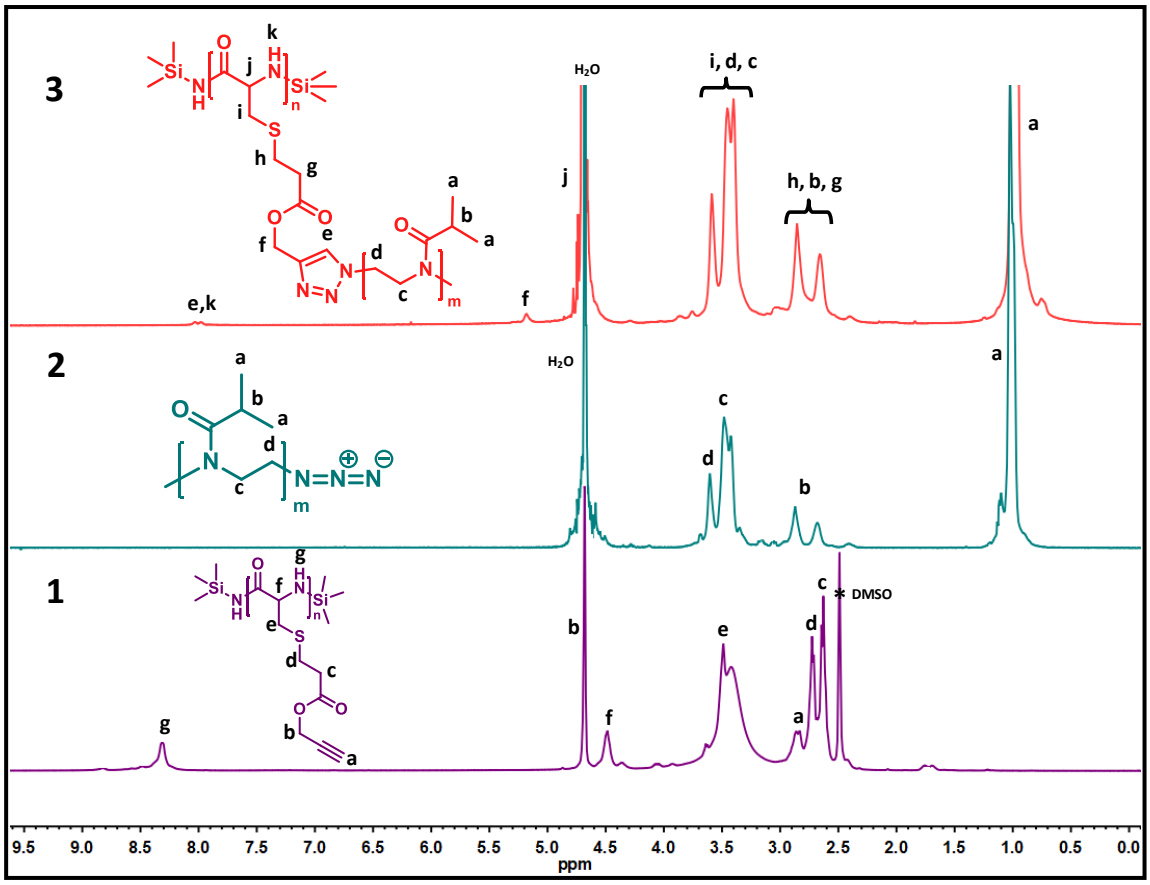

Figure S8. ^{1}H-NMR spectra of **C1** in DMSO-d_6 (1), **P1** (2) and **G1** (3) in D_2O.

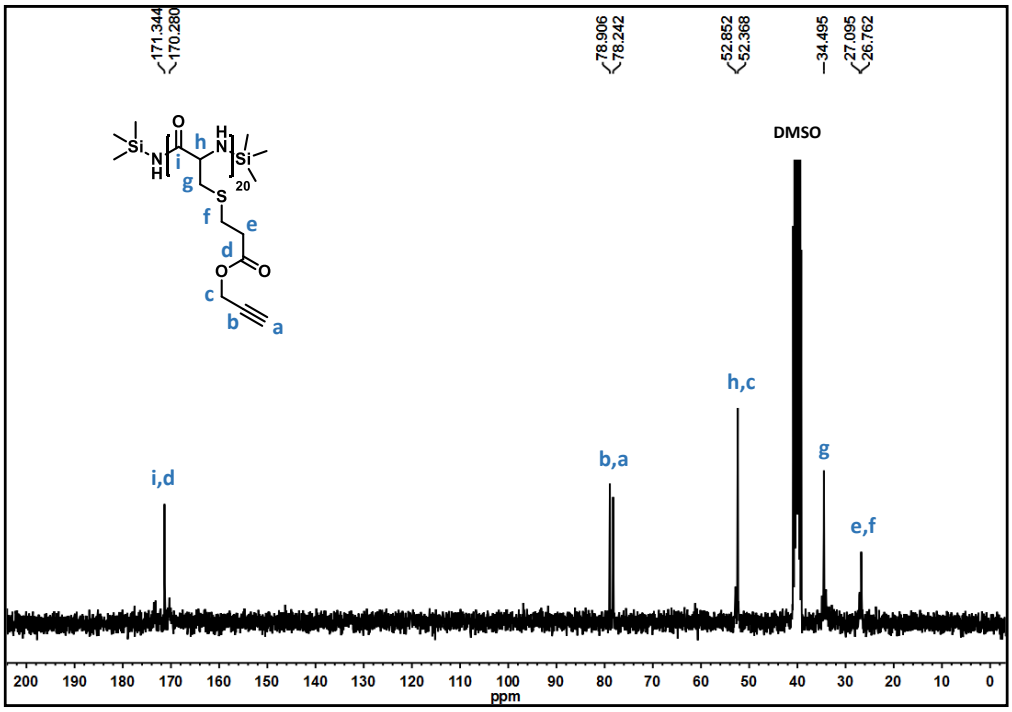

Figure S9. ^{13}C-NMR spectrum of PCys-S-Pr (**C1**) in DMSO-d_6

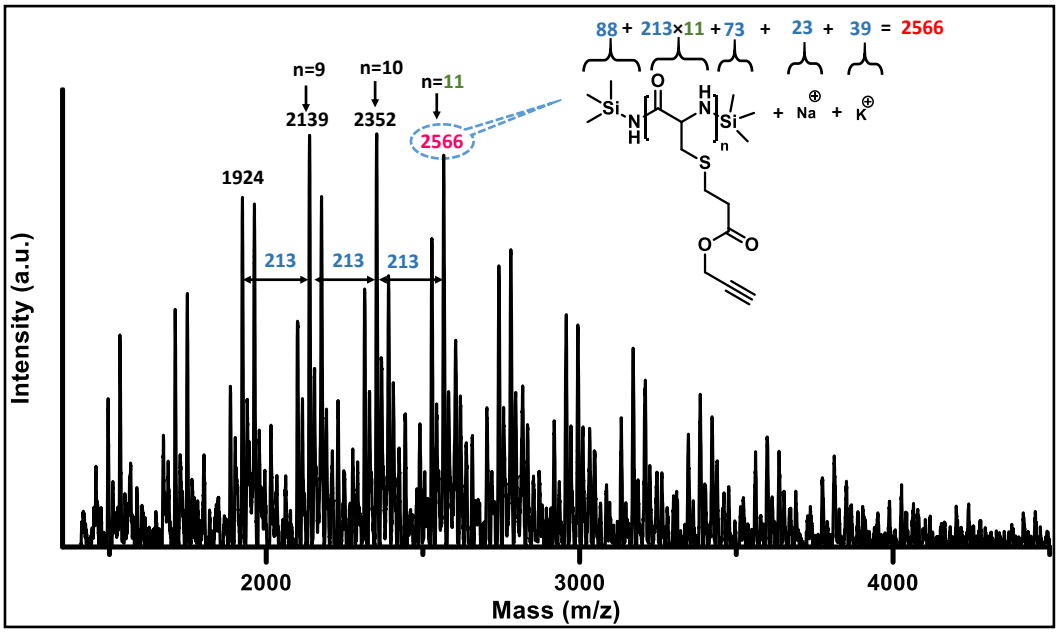

Figure S10. MALDI-TOF-MS spectrum of PCys-S-Pr (**C1**).

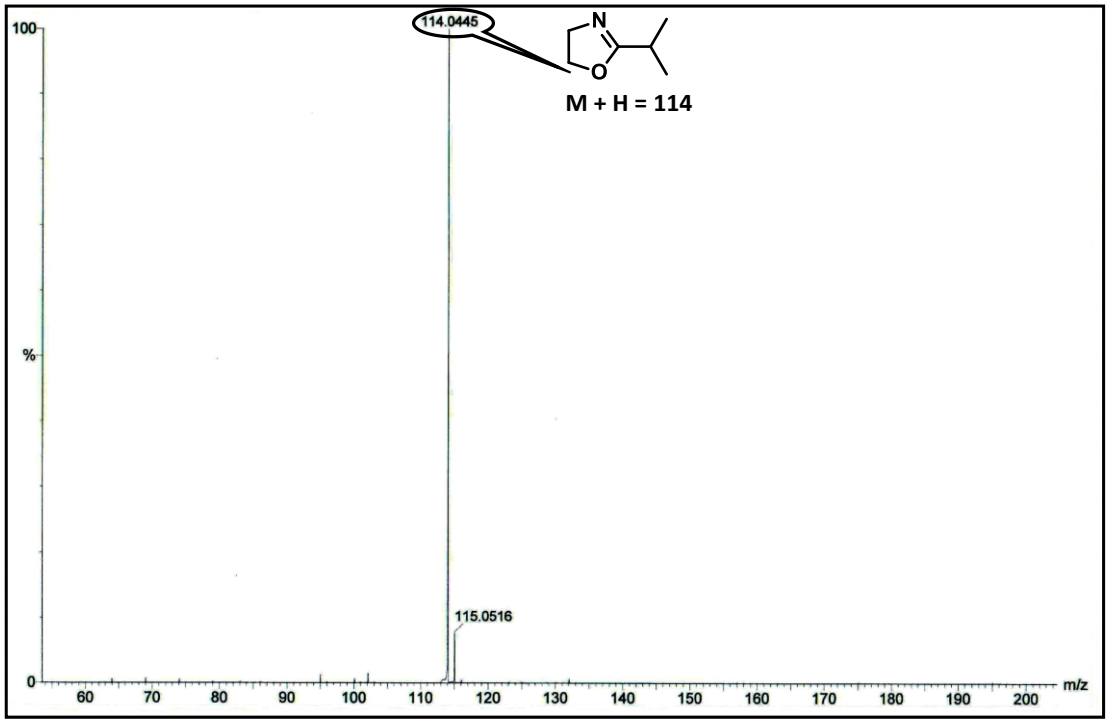

Figure S11. ESI-MS spectrum of ^{i}POx in DCM

ESI-MS$_{i\text{POx}}$: m/z (%) = 114.0445 (100) ($M+1H^{+}$)

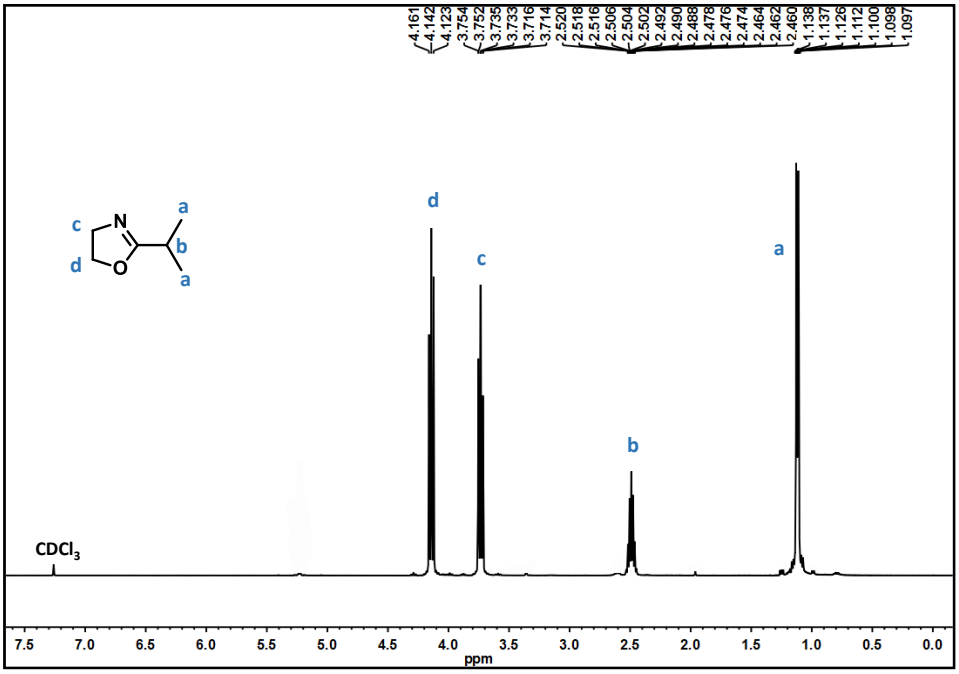

Figure S12. ^{1}H-NMR spectrum of ^{i}POx in $CDCl_3$

^{1}H NMR (500 MHz, $CDCl_3$, TMS) δ (ppm): 4.14 (m, 2H), 3.73 (m, 2H), 2.49 (m, 1H), 1.12 (m, 6H)

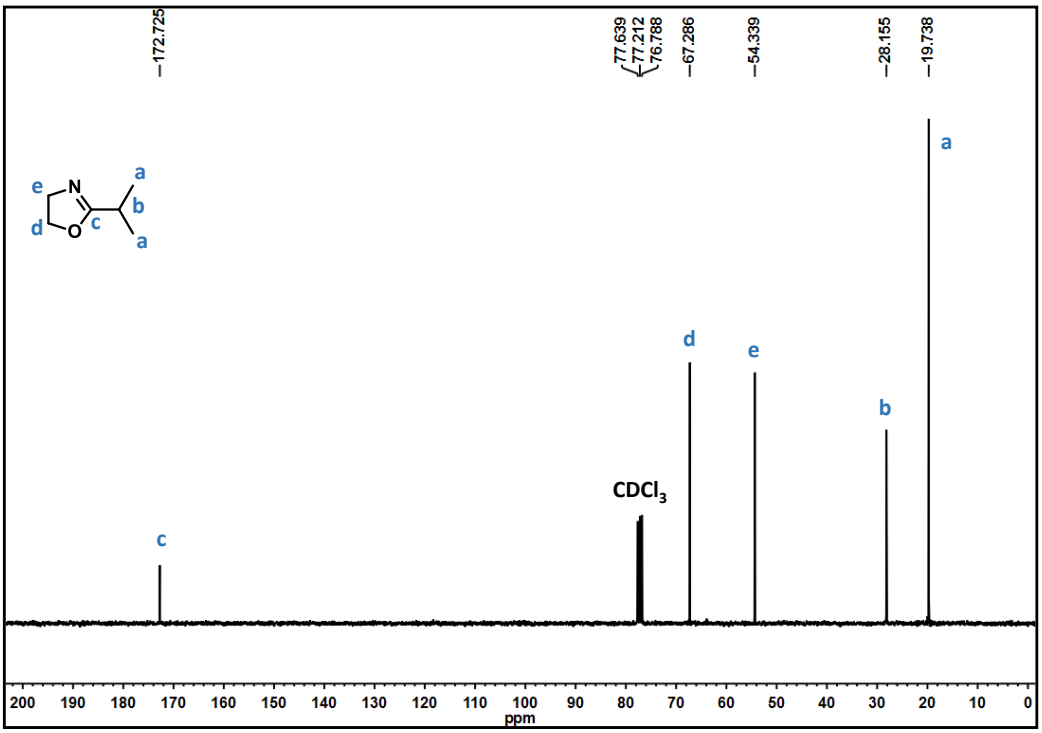

Figure S13. ^{13}C-NMR spectrum of ^{i}POx in $CDCl_3$

^{13}C-NMR (300 MHz, $CDCl_3$, TMS) δ (ppm): 19.738, 28.155, 54.399, 67.286, 172.725

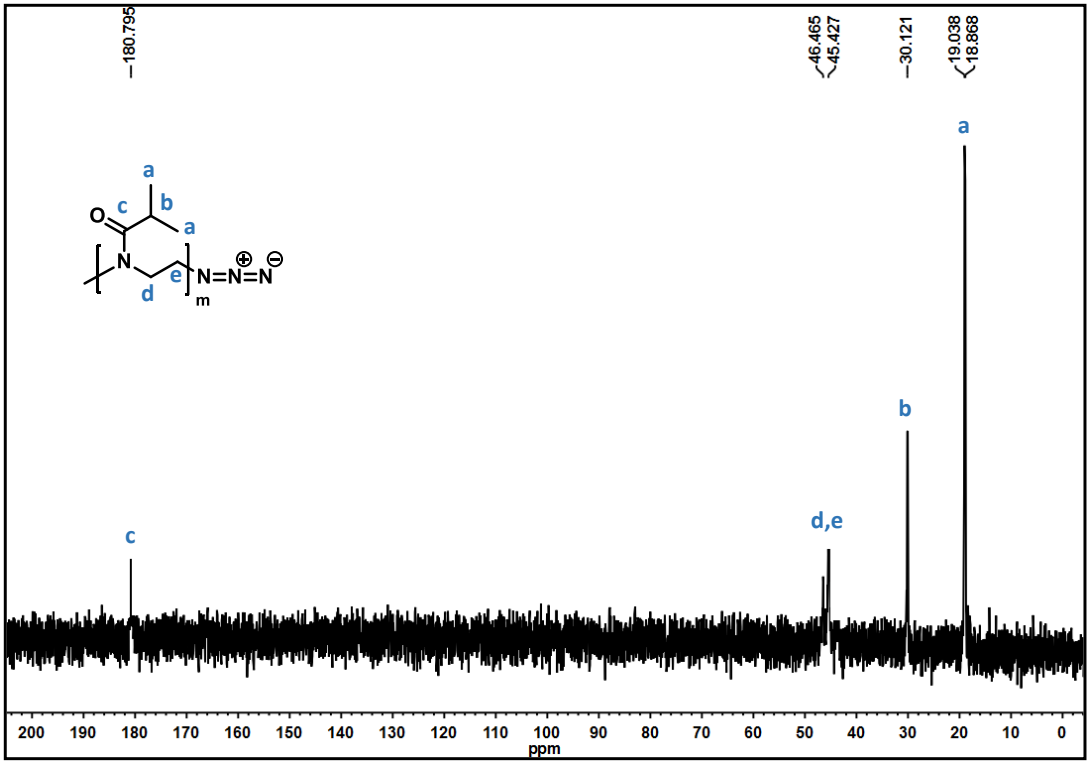

Figure S14. ^{13}C-NMR spectrum of P^{i}POx (**P1**) in D_2O

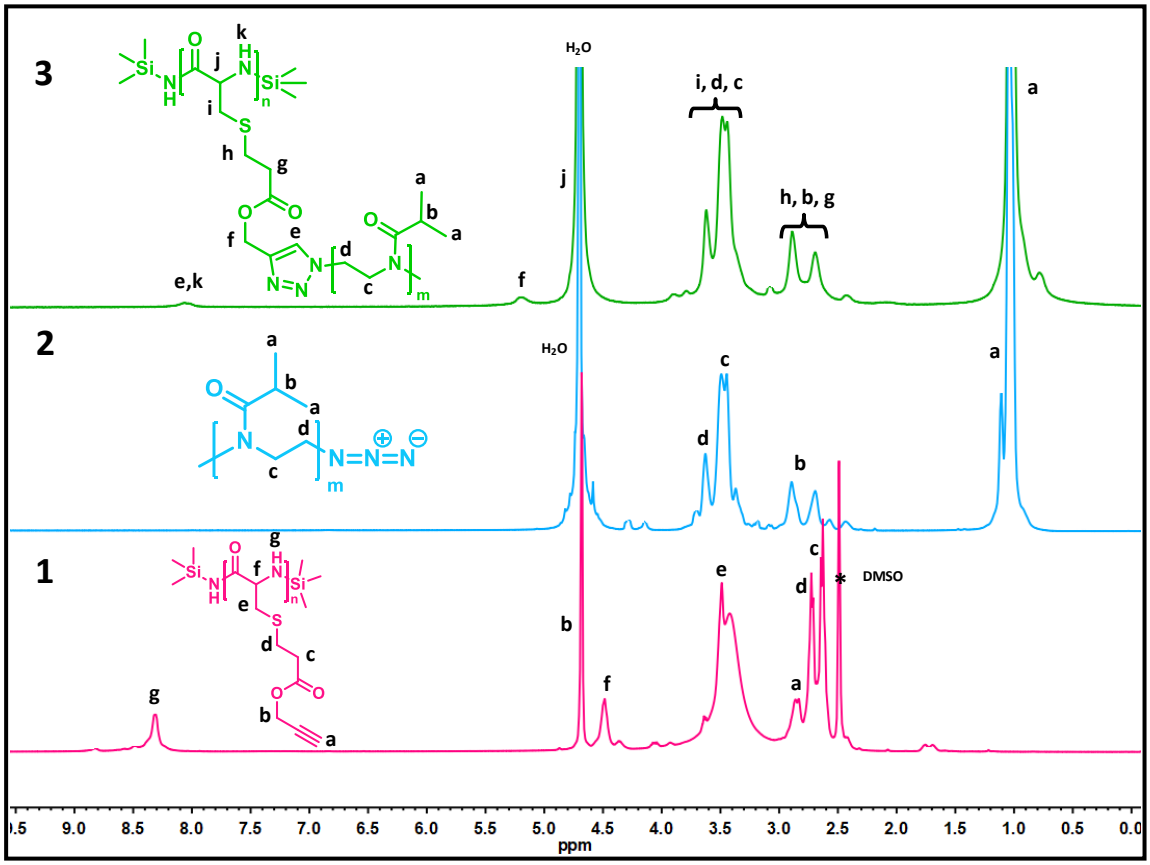

Figure S15. ^{1}H-NMR spectra of **C1** in DMSO-d_6 (1), **P2** (2) and **G2** (3) in D_2O

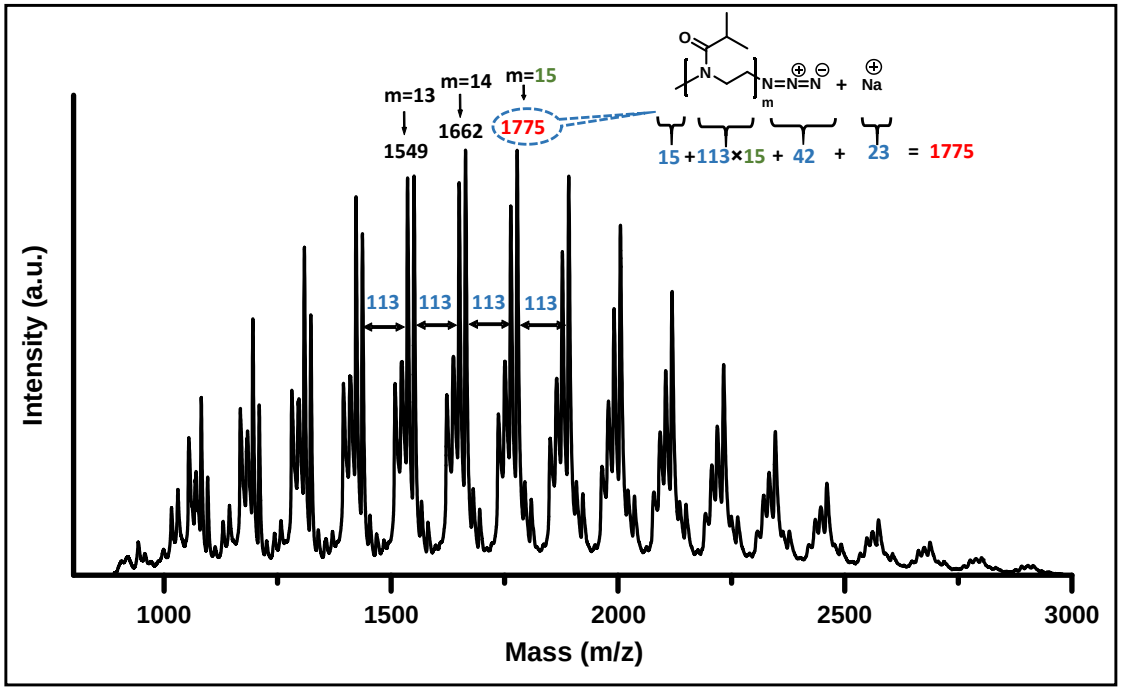

Figure S16. MALDI-TOF-MS spectrum of **P1**

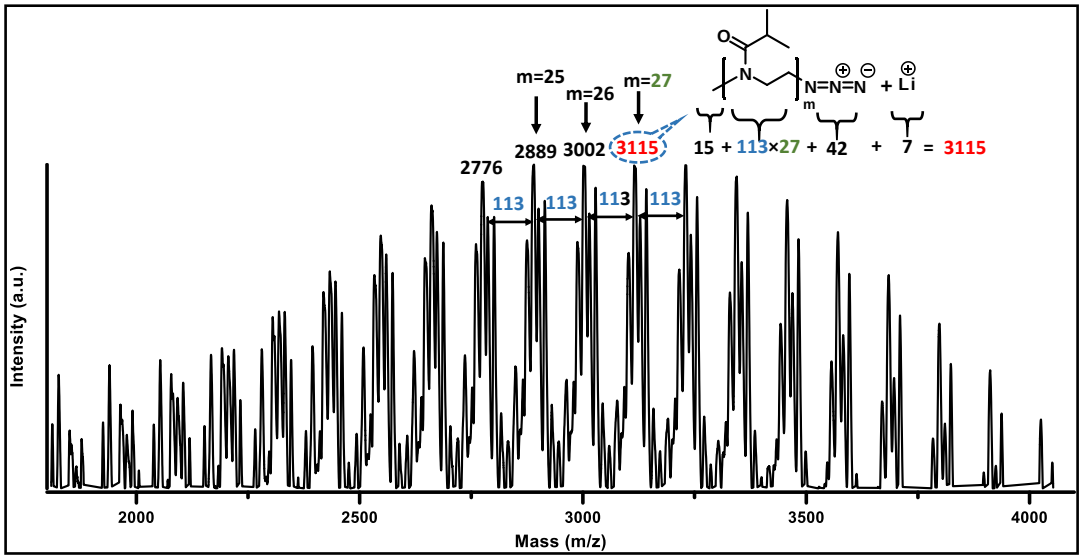

Figure S17. MALDI-TOF-MS spectrum of **P2**

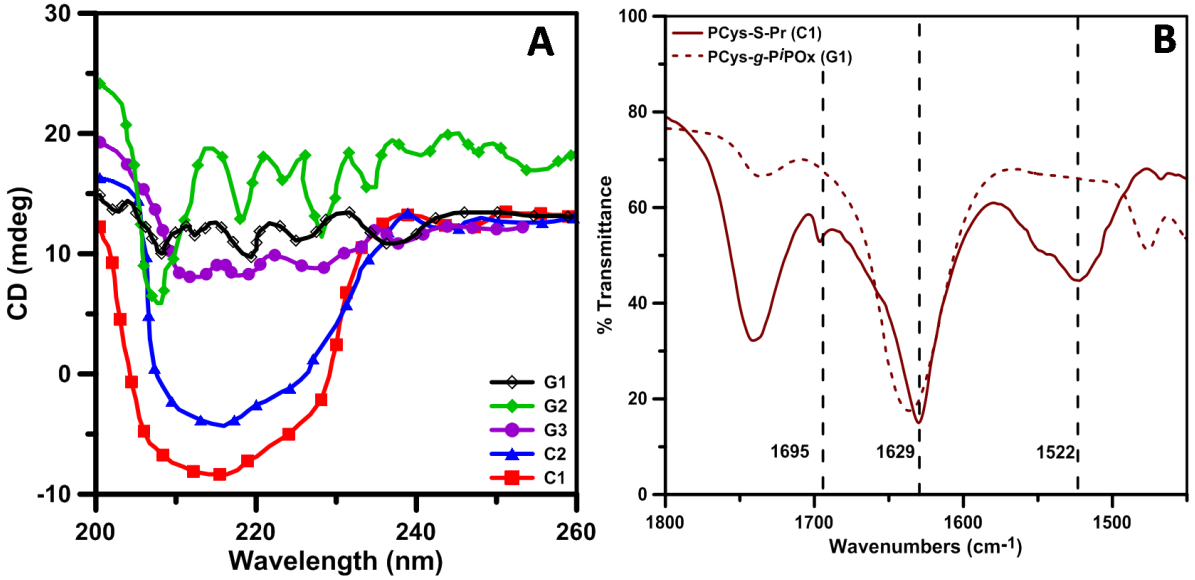

Figure S18. CD spectrum of different synthesized compounds in DMF (A) and FTIR spectra showing band positions of different amide regions (B)

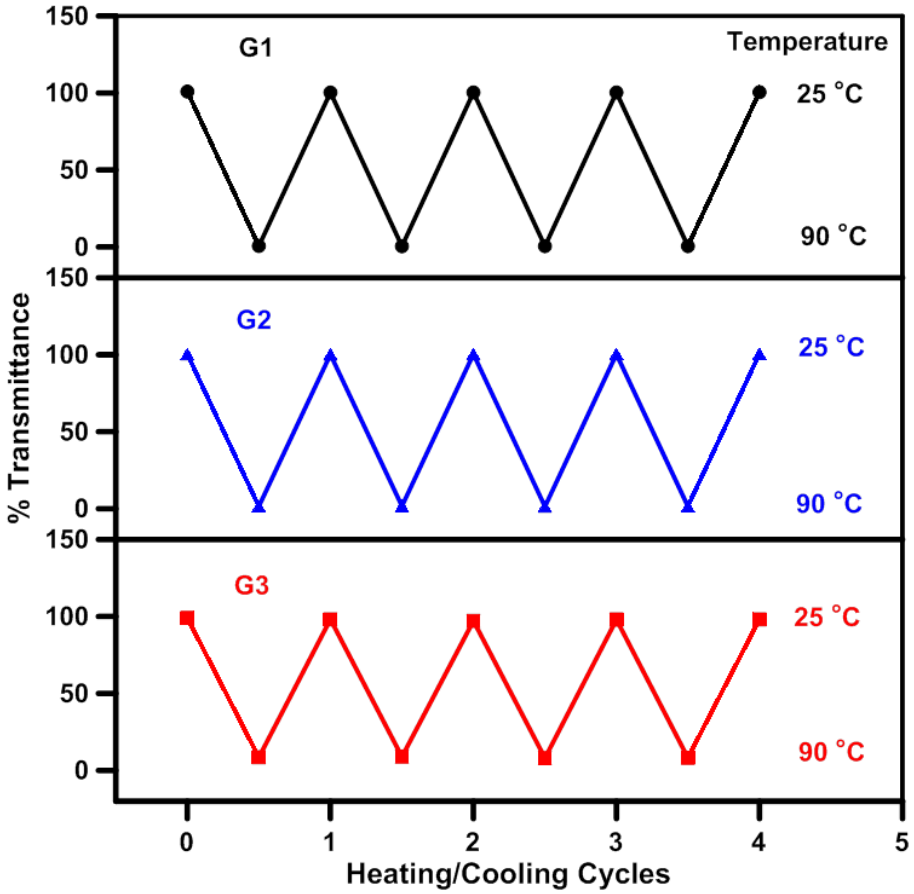

Figure S19. Temperature dependent % transmittance of aqueous PCys-*g*-P^{i}POx samples (0.2 wt%) during heating/cooling cycles. Each data point was obtained after equilibrating the sample solution at a particular temperature for 5 min.

Determination of critical aggregation concentration (CAC)

Pyrene was used as the polarity probe for determination of CAC. Pyrene is a well-known dye to investigate the polarity changes in the microenvironment (micelle or vesicle) from polarity changes in the macroenvironment (bulk solvent) A characteristic property of pyrene, which indicates the polarity of the environment in which it is solubilised, is the ratio of its fluorescence peaks at $\lambda \approx 372$ nm for the 0–0 band (I_1) and at $\lambda \approx 383$ nm corresponds to the third principal vibronic band (I_3) in water, which are very much sensitive to polarity of the medium. For this a series of polymer sample (**G2**) solutions in water was prepared of concentration ranging from 1 mg/mL to 1×10^{-2} mg/mL. A stock solution of pyrene of 10^{-4}(M) in acetone was prepared and 20 μL of that solution was transferred into 9 separate glass vials. After evaporating the acetone, 2mL of each polymer solution was added into those vials separately and sonicated for 10 minutes and kept for overnight undisturbed. Final concentration of pyrene was kept constant at 10^{-6}(M) for each solution. Fluorescence emission intensity was measured by exciting those solutions at $\lambda \approx 334$ nm and keeping the slit width at 5 nm. After normalising the intensity at $\lambda \approx 372$ nm, the ratio of I_{383} and I_{372} (I_3/I_1) was plotted against the logarithm of the concentration (mg/mL) of different polymer solutions. The plot of intensity ratio (I_3/I_1) against the log of polymer concentration (mg/mL) showed a slow increase of the I_3/I_1 value with concentration followed by a sudden jump. The CAC was obtained from the interception point of two straight lines and was found to be 0.22 mg/mL (Figure S20).

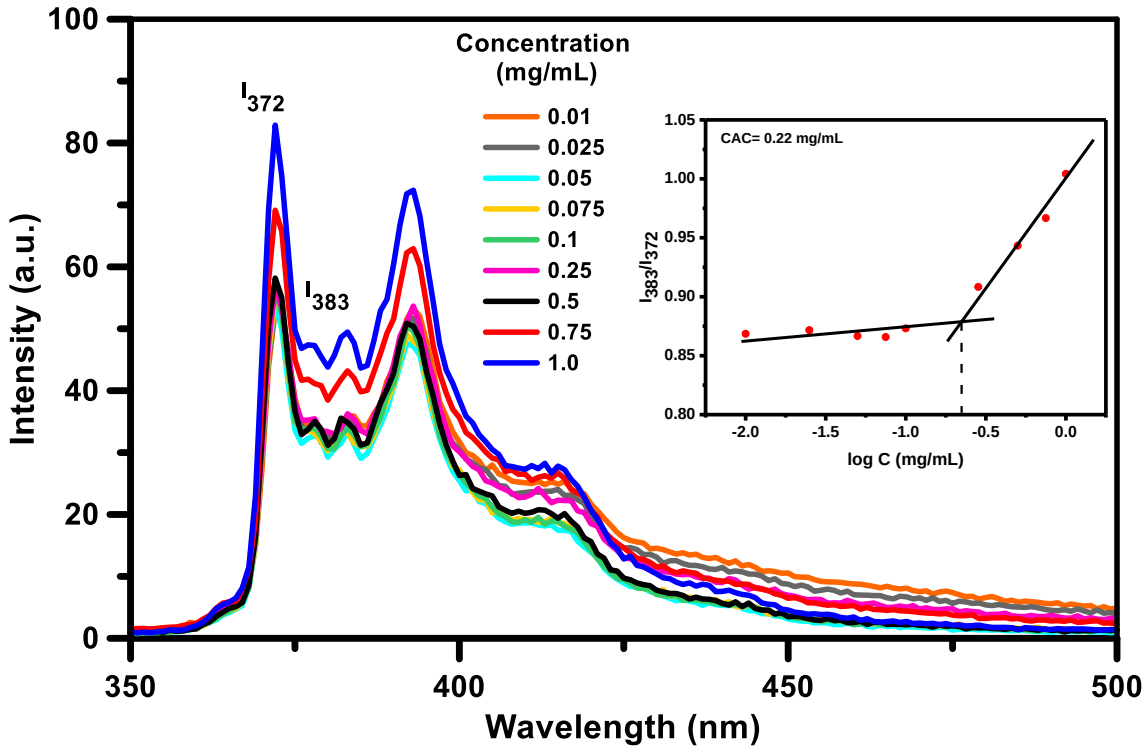

Figure S20. Emission spectra of pyrene (λ_{ex} = 334 nm) in the presence of aqueous **G2** of varying concentration. Inset represented the plot of fluorescence vibronic intensities ratio (I_3/I_1) as a function of the **G2** concentration as measured from emission spectra.

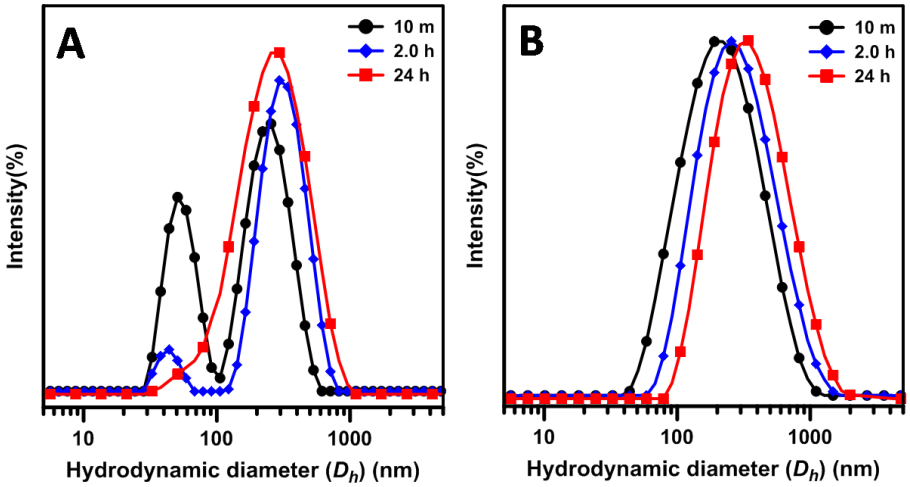

Figure S21: Time dependent intensity-weighted particle size distributions of **G3** in water at a concentration of 2.0 (A) and 5.0 (B) mg/mL, as obtained from DLS.

Table S1. Particle size distribution of the graft copolymers (**G1**, **G2** and **G3**) in water at different time intervals as observed from DLS, showing particles of mainly two different size distributions.

Time interval	Graft copolymers														
	Particle size distribution (G1)					Particle size distribution (G2)					Particle size distribution (G3)				
	Small (nm)	St. dev.	Large (nm)	St. dev.	PDI	Small (nm)	St. dev.	Large (nm)	St. dev.	PDI	Small (nm)	St. dev.	Large (nm)	St. dev.	PDI
0.0 h	20.1	9.9	195	52.5	0.384	16	3.6	237	25.9	0.330	40	2.8	294	56.3	0.303
2.0 h	21.2	10.8	244	83.4	0.345	19.5	6.1	221	71.8	0.256	37.8	5.3	294.7	64.3	0.287
6.0 h	17.6	11.8	246.2	58.3	0.321	22.4	5.9	250.2	74.3	0.282	41.2	8.3	292	66.1	0.354
10 h	19.5	8.4	285	69.7	0.338	19.7	3.0	293.8	51.1	0.485	37.8	5.3	302.1	78.6	0.351
15 h	21.7	8.3	302.9	45.9	0.379	27.0	2.1	302.4	53.4	0.343	43.18	2.6	302.4	61.1	0.370
20 h	20.8	9.7	309.4	55.30	0.415	25.0	11.7	299.7	61.1	0.370	36.2	5.2	300.9	53.4	0.456
24 h	20.3	7.3	323.1	41.5	0.342	24.2	5.2	334	53.4	0.421	31.7	5.9	304	50.7	0.434

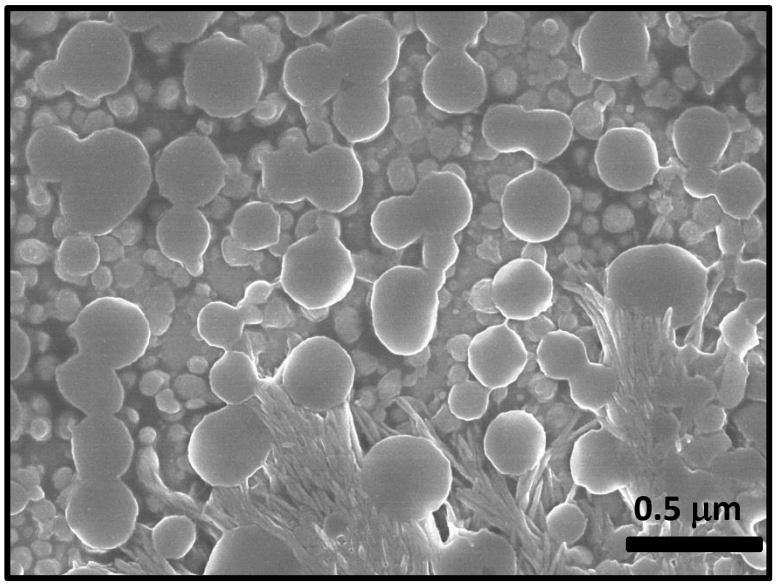

Figure S22. FESEM image of **G2** in water showing unit vesicles with an average diameter ~ 20 nm and conjugate vesicles with an average diameter of ~250 nm.

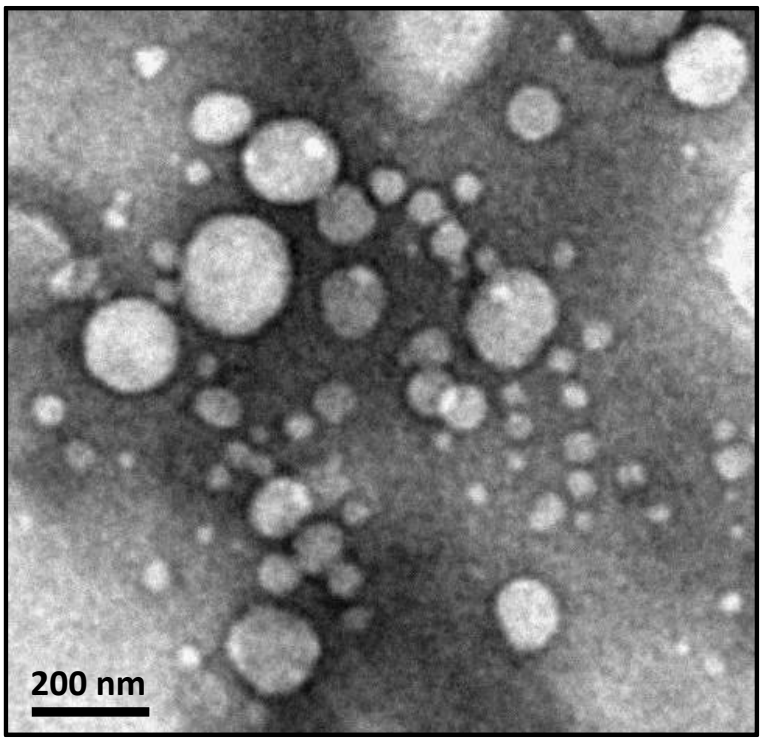

Figure S23. TEM image of **G3** solution in water showing unit vesicles (avg. diameter ~ 15 nm) and conjugate vesicles (avg. diameter ~ 170).

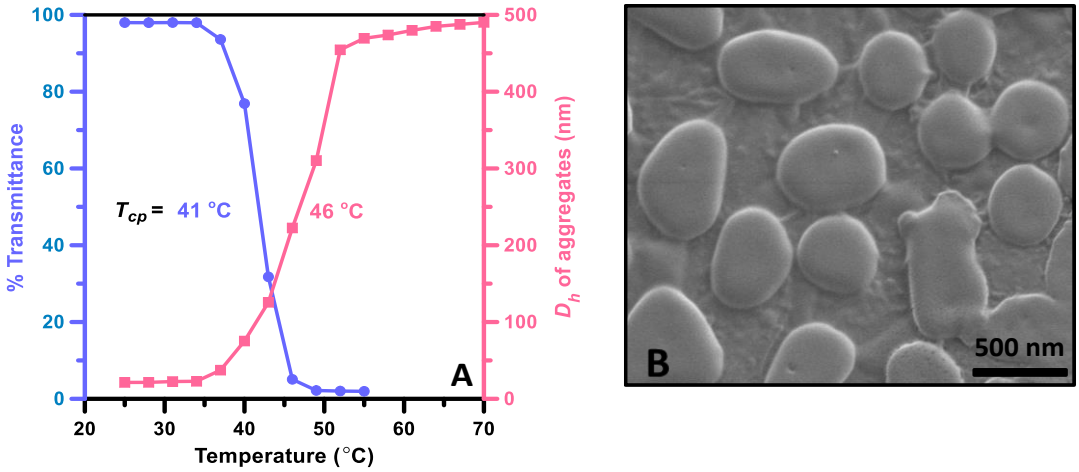

Figure S24. (A) Average hydrodynamic diameter of **G2** (0.2 wt%, H_2O) vs temperature plot (pink) as measured from DLS. Also the correlation between hydrodynamic diameters (D_h)s (■) and % transmittance (at λ = 500 nm) (●) of aqueous **G2** solution (0.2 wt%) at different temperatures showing prominent cloud points of **G2** and (B) FESEM image of aggregated morphology of **G2** (0.2 wt %) in water above its T_{cp} (41 °C).

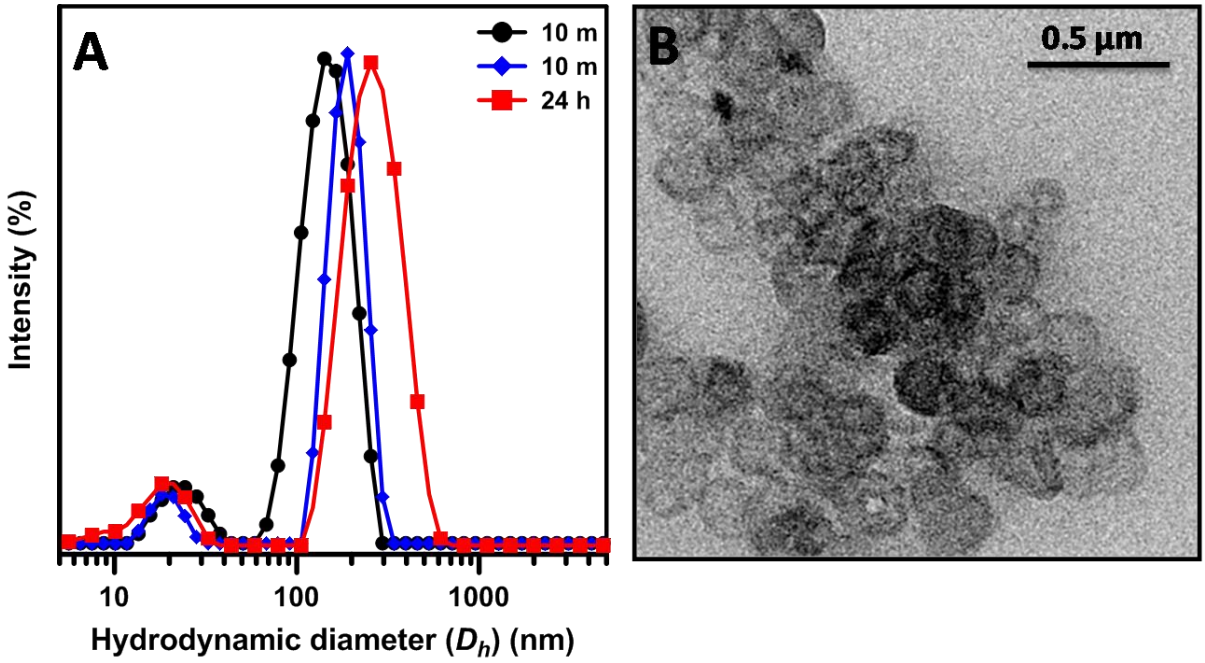

Figure S25. DLS curves (A) and TEM image (B) of **G2** vesicles in DCM (0.1 wt%).

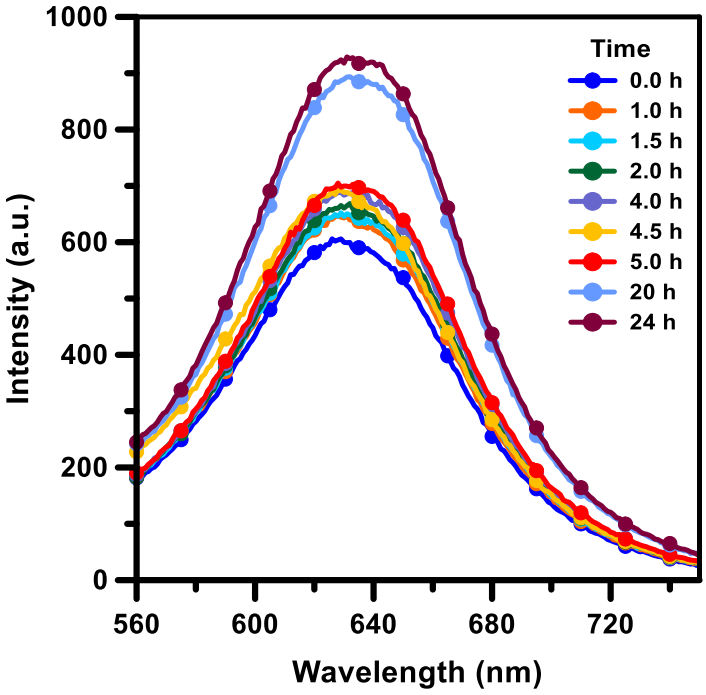

Figure S26. Emission spectra of NR in water at different time intervals in the presence of 0.2 wt% of **G2**.

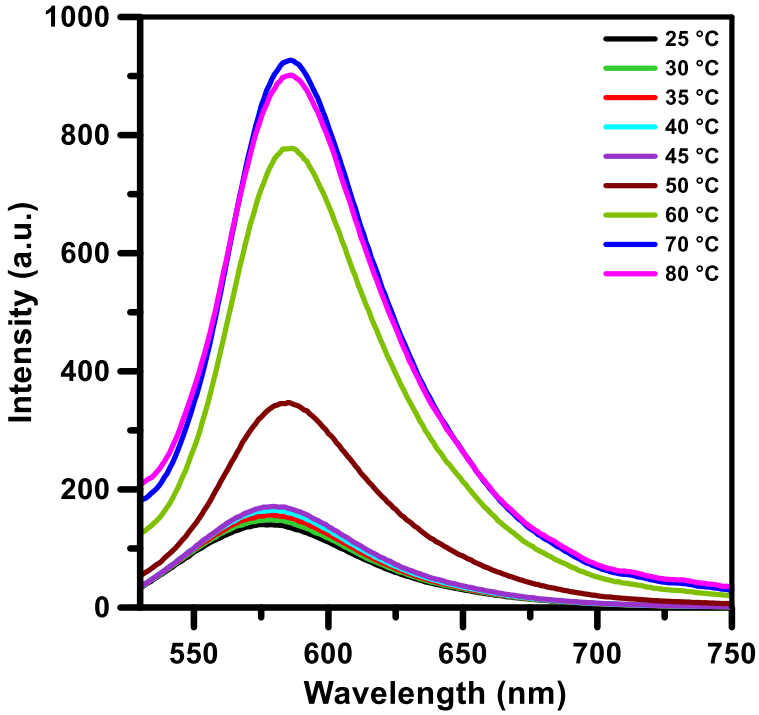

Figure S27. Emission spectra of EB-encapsulated **G1** vesicle at different temperatures showing increment in intensity with increasing solution temperature.

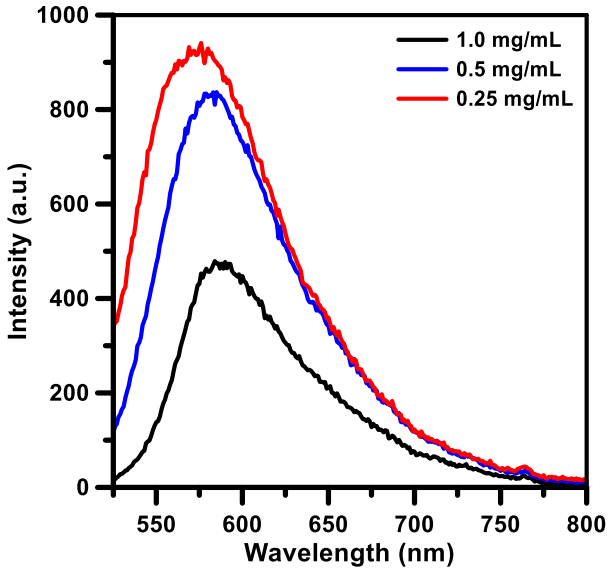

Figure S28. Emission spectra of neat EB in water showing increment in intensity upon dilution.

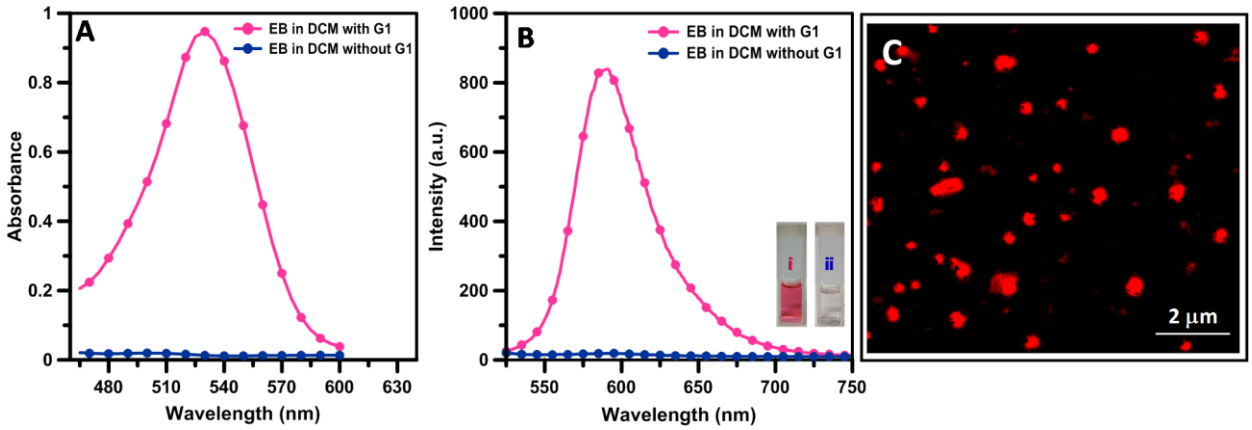

Figure S29. (A) UV-vis spectra of free EB and EB-encapsulated **G1** in DCM; (B) Emission spectra (λ_{max}= 590 nm) of free EB and EB-encapsulated **G1** in DCM and inset showed difference of colour intensity of the EB in DCM with (i) and without (ii) 0.2 wt% of **G1** and (C) Fluorescence confocal microscopic image of EB-loaded **G1** vesicles in DCM.

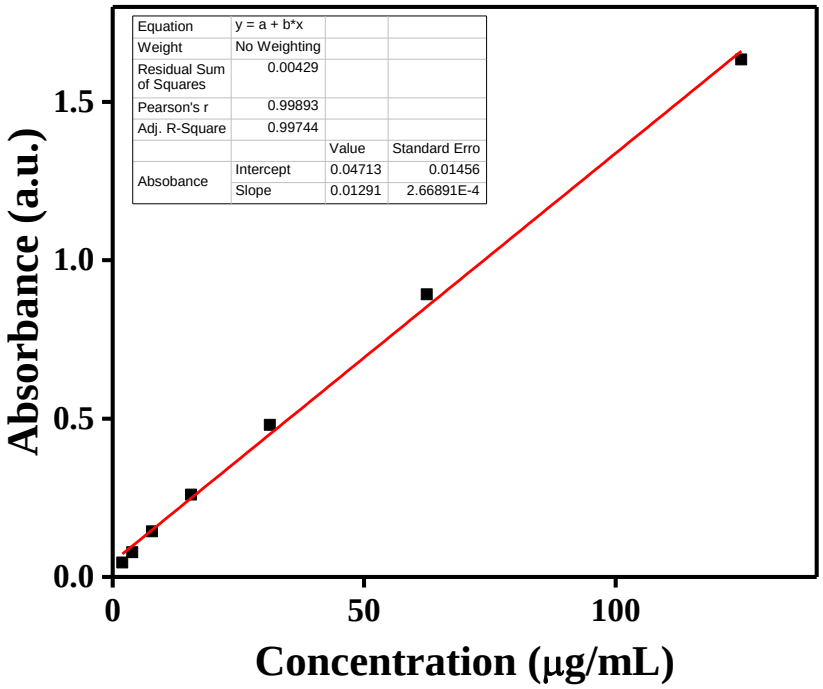

Figure S30. Calibration curve of neat Dox in water

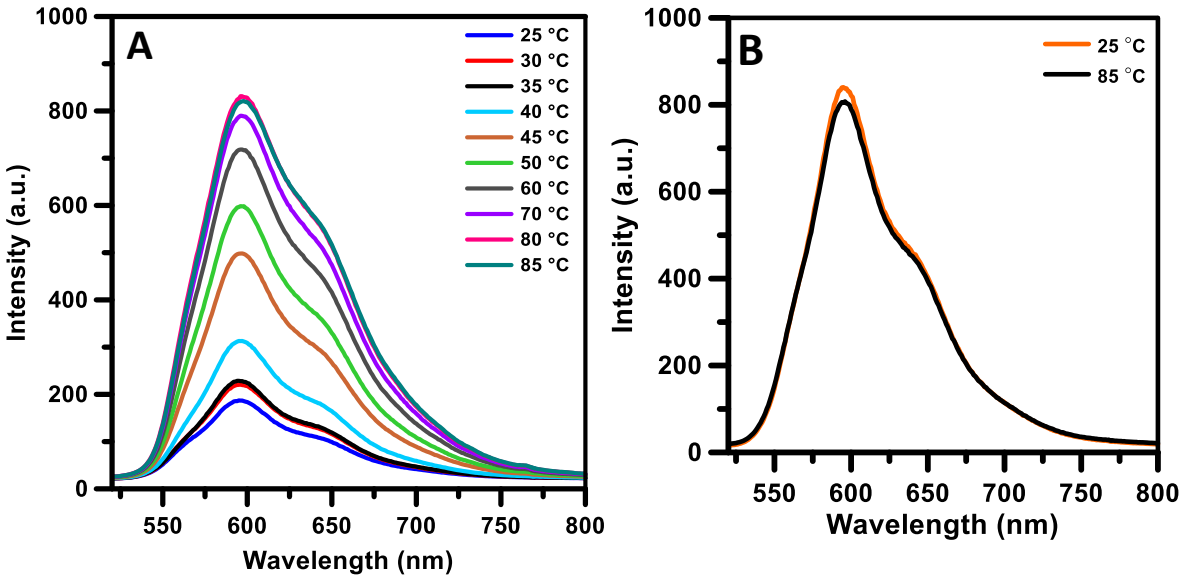

Figure S31. Fluorescence emission spectra of Dox-loaded vesicle (**G2**) as a function of increasing temperature from 25 to 85 °C (A) and fluorescence emission spectra of free Dox in water at two extreme temperatures showing no such change in intensity (B).

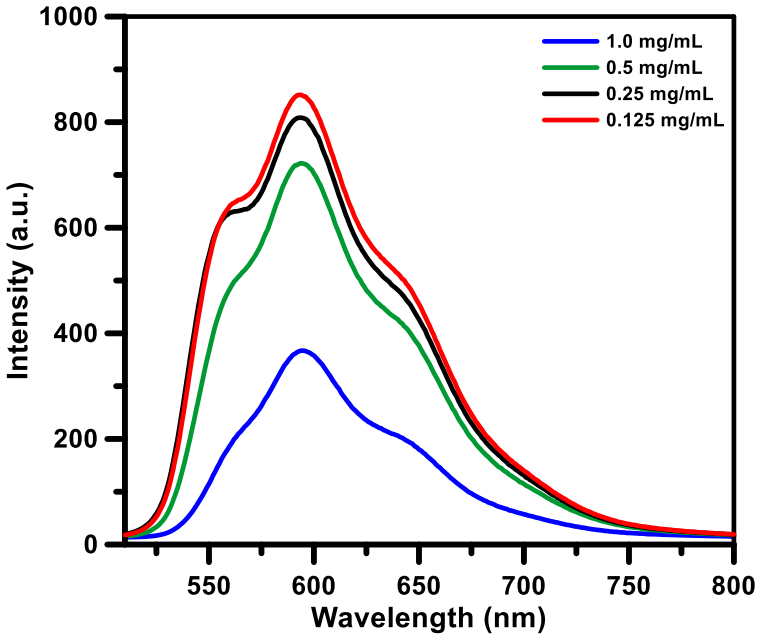

Figure S32. Emission spectra of neat Dox in water showing increment in intensity upon dilution.

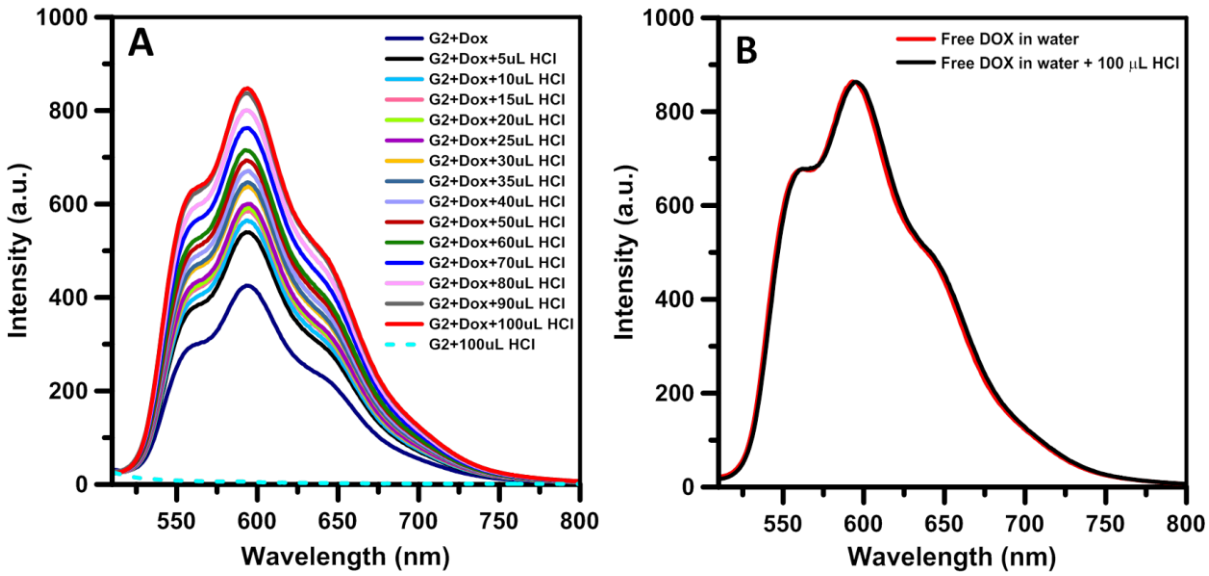

Figure S33. Fluorescence emission spectra of Dox-loaded vesicles (**G2**) suspensions after treated with HCl of varying concentrations (A) and Fluorescence emission spectra of neat Dox in water in the presence of concentrated HCl (12 N) showing no such change in intensity (B).

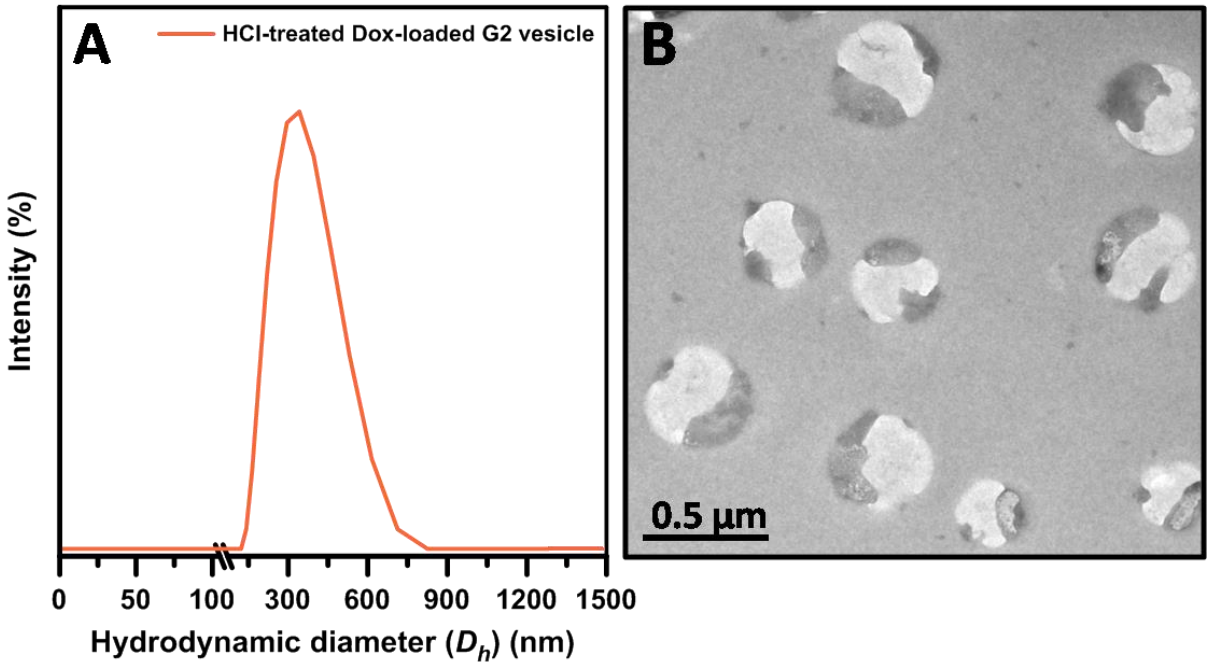

Figure S34. Dox-loaded **G2** vesicles after treated with HCl: (A) DLS data and (B) TEM image.

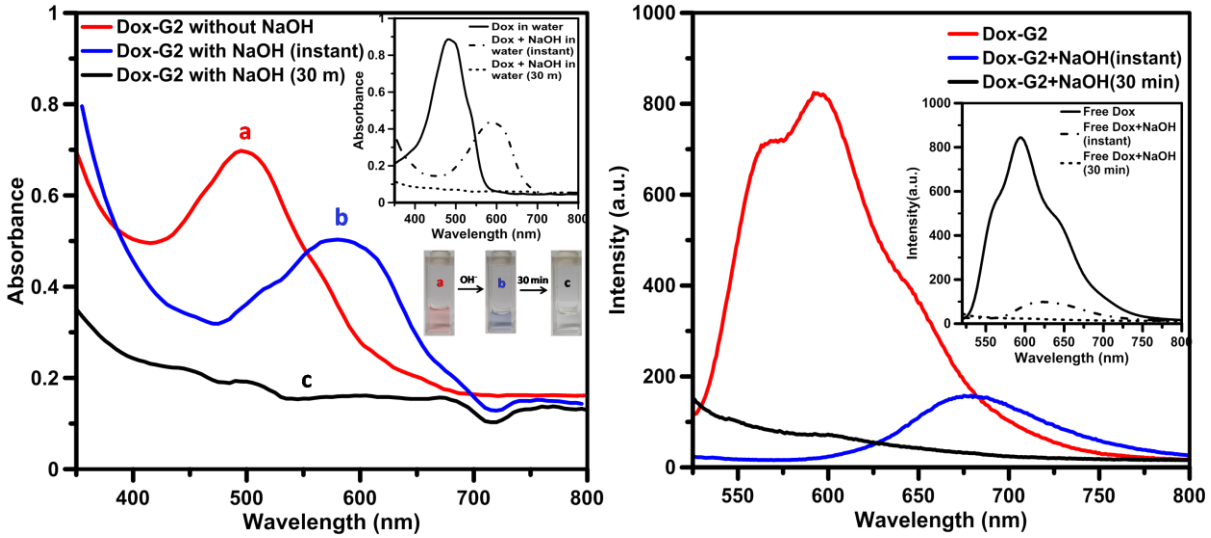

Figure S35. (A) Absorption spectra of Dox encapsulated in **G2** along with its base (NaOH) treated solution. Inset showed its colour change and the results of control experiment of free Dox in presence of base. (B) Emission spectra of Dox encapsulated in **G2** along with its base (NaOH) treated solution. Inset showing results of control experiment of free Dox in presence of base (NaOH).

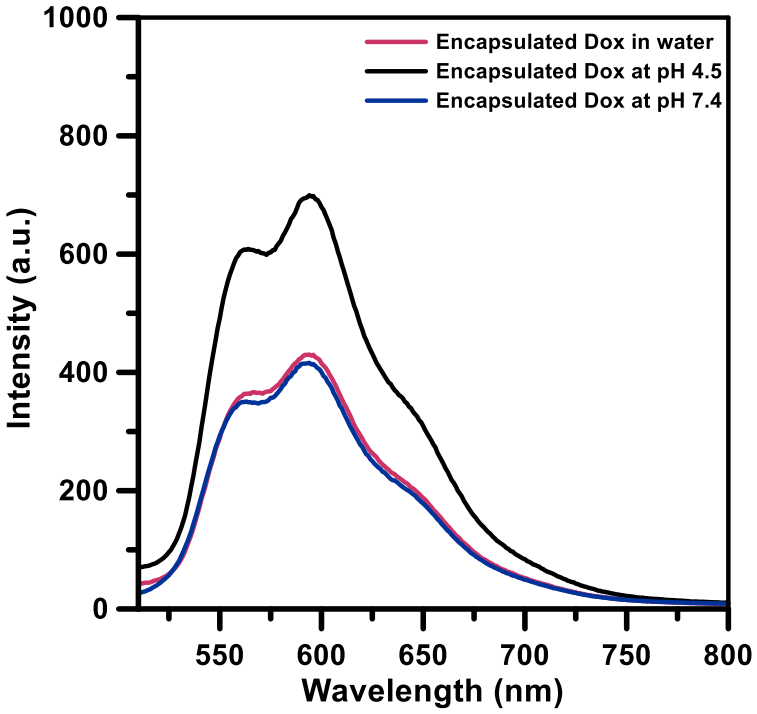

Figure S36. Emission spectra of Dox encapsulated in **G2** in phosphate buffer solution at two different pHs (4.5 and 7.4) at 37 °C.